All-Cellulose Cryogels with Tunable Extracellular Matrix-Mimetic Architecture

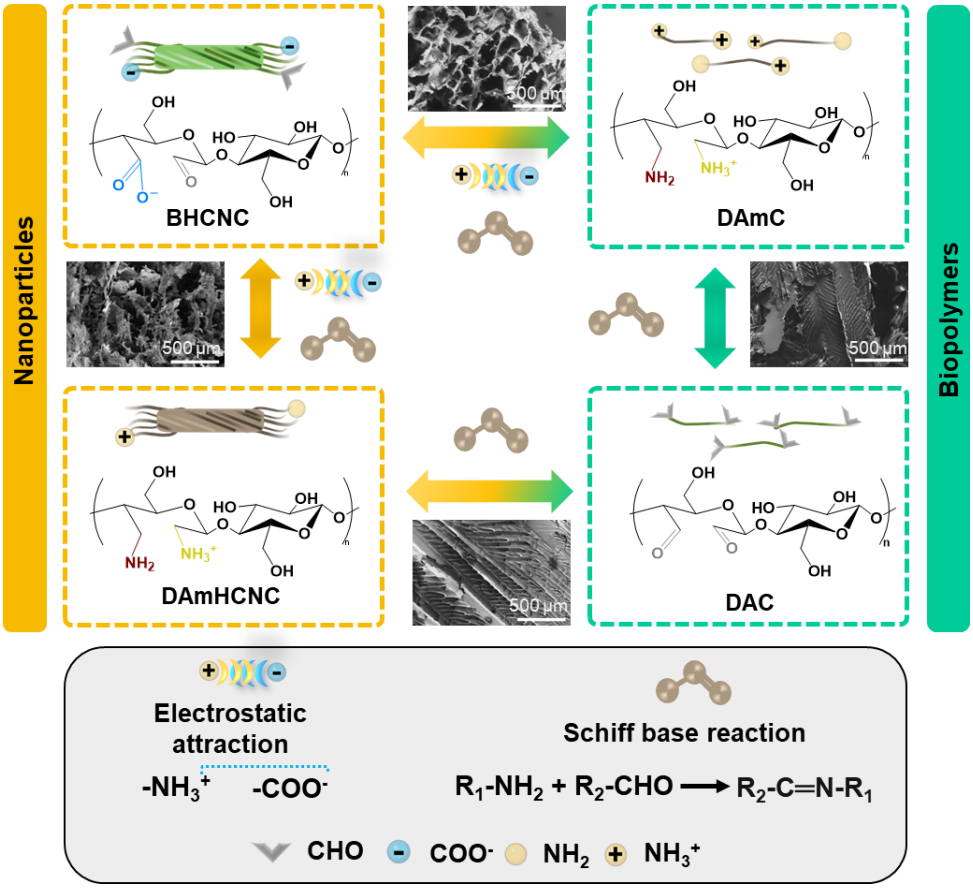
2025 *BioResources* Early Career Investigator Award Winner

Lucas Lawrence Franz,[a] Karolina Patricia Akelaitis,[a] Neela Nicole Cooper,[a] Sina Kheirabadi,[a] Mica L. Pitcher,[a,b] Jeff Lin,[a] Mitra Ann Salari,[a] Anjali Kiran Baikerikar,[a] Suchitra Thirumalai,[a] Roya Koshani ,[a] and Amir Sheikhi [a,b,c,d,e,*]

** Corresponding author: sheikhi@psu.edu*

DOI: 10.15376/biores.21.3.6416-6435

GRAPHICAL ABSTRACT



All-Cellulose Cryogels with Tunable Extracellular Matrix-Mimetic Architecture

2025 *BioResources* Early Career Investigator Award Winner

Lucas Lawrence Franz,[a] Karolina Patricia Akelaitis,[a] Neela Nicole Cooper,[a] Sina Kheirabadi,[a] Mica L. Pitcher,[a,b] Jeff Lin,[a] Mitra Ann Salari,[a] Anjali Kiran Baikerikar,[a] Suchitra Thirumalai,[a] Roya Koshani ,[a] and Amir Sheikhi [a,b,c,d,e,*]

The hierarchical structure of an extracellular matrix (ECM) regulates cell behaviors, including adhesion, proliferation, migration, and differentiation. Inspired by this principle, tunable all-cellulose cryogels were engineered that partially mimic the architecture of native tissue microenvironments. Building upon the authors' recent advances in hairy cellulose nanocrystals (HCNC) with finely tuned chemical functionalities and nanoarchitectures, this work leverages amine- and aldehyde-functionalized HCNC together with polymeric cellulose derivatives as building blocks to develop cryogels with organ-specific, ECM-like architectures. Schiff base reactions in conjunction with electrostatic attraction mediate the formation of dynamic covalent networks that self-assemble into hydrogels, which are subsequently lyophilized to yield porous cryogels. Variations in the composition and functionality of cellulosic building blocks govern scaffold architecture by modulating network connectivity, enabling the regulation of pore features. This work establishes a sustainable, non-animal-derived material platform that may bridge biomass nanotechnology and regenerative medicine, demonstrating how renewable, functionally engineered cellulose across micro- and nanoscale can be translated into next-generation biomimetic scaffolds.

DOI: 10.15376/biores.21.3.6416-6435

Keywords: Hairy nanocellulose; Biomimetic materials; Sustainable biomaterials; Tissue engineering

*Contact information: a: Department of Chemical Engineering, The Pennsylvania State University, University Park, PA 16802, USA; b: Department of Chemistry, The Pennsylvania State University; c: Department of Biomedical Engineering, The Pennsylvania State University; d: Huck Institutes of the Life Sciences, The Pennsylvania State University, USA; e: Department of Neurosurgery, College of Medicine, The Pennsylvania State University; *Corresponding author: sheikhi@psu.edu*

INTRODUCTION

Living tissues comprise hierarchical structures of cell assemblies and extracellular matrices (ECM) that together enable specialized mechanical behavior and dynamic responsiveness (Fang *et al.* 2020). ECM is a complex, three-dimensional (3D) network that provides cells with essential structural support and biophysicochemical cues, regulating cell behaviors, such as adhesion, proliferation, migration, and differentiation (Yamada *et al.* 2022; Zhao *et al.* 2025). The multiscale organization of native ECM, spanning from nanoscale protein fibrils (*e.g.*, collagen) to microscale fiber bundles and macroscale porosity, is crucial for regulating mechanical properties and guiding cell mechano-transduction, which are fundamental to tissue homeostasis and regeneration (Sun 2021;

Bock *et al.* 2025). Accordingly, a major challenge in regenerative medicine, particularly for wound healing, is engineering scaffolds that recapitulate the tissue-mimetic hierarchical ECM architecture using cytocompatible materials (Chen *et al.* 2024).

Tissue- or ECM-mimetic scaffolds typically require interconnected porous networks that support nutrient diffusion, oxygen transport, and cell infiltration, with pore sizes in biologically relevant ranges (*e.g.*, tens to hundreds of micrometers, depending on tissue type), along with mechanically stable yet compliant architectures that maintain structural integrity during tissue regeneration (Hollister 2005; Jaberi *et al.* 2025). In this work, the term 'ECM-mimetic' refers to the reproduction of these structural characteristics, specifically organization, interconnected porosity, and tunable network architecture, using cellulose-based cryogels.

Cellulose has emerged as a promising sustainable polymer owing to its abundance in the world, robust mechanical strength, dose-dependent biocompatibility, and a high density of hydroxyl groups that enable versatile chemical modifications (Habibi *et al.* 2010; Pitcher *et al.* 2024). There has been remarkable interest in using plant-derived materials to develop new, green scaffolds to replace animal-derived counterparts, such as collagen and gelatin. This shift, although challenging, may minimize concerns related to zoonotic pathogen transmission and immunogenicity, and provide more sustainable and cost-effective source materials (Badylak and Gilbert 2008; Modulevsky *et al.* 2016). This work builds on hairy cellulose nanocrystals (HCNC), a specialized form of nanocellulose characterized by a crystalline core and flexible disordered cellulose chains ("hairs") (van de Ven and Sheikhi 2016). HCNC have up to an order-of-magnitude higher functional group density than conventional CNC, which has only a crystalline core. Thus, HCNC exhibit improved physicochemical assembly and network connectivity (Sheikhi and van de Ven 2017).

Colloidal and polymeric cellulose derivatives have been previously used to fabricate hierarchically structured cellulosic cryogels (Amini *et al.* 2025; Koshy *et al.* 2025), in conjunction with physical (Shakya *et al.* 2024) or chemical (Yang and Cranston 2014; Chau *et al.* 2016) crosslinking approaches. Chemical crosslinking offers a route to develop more mechanically stable aerogels with tunable structural properties without significantly compromising surface area (De France *et al.* 2017). When combined, amine- and aldehyde-bearing cellulose derivatives undergo a reversible nucleophilic condensation reaction to form imine bonds *via* Schiff base crosslinking (Wang *et al.* 2025). It is hypothesized that by varying the aldehyde-to-amine (–CHO:–NH_2) molar ratio of cellulose derivatives and leveraging physical interactions such as electrostatic attraction and chain entanglement, HCNC and biopolymeric cellulose derivatives can assemble into stable hydrogel networks, which yield freestanding cryogels with ECM-like pore architectures *via* subsequent freeze-drying.

In this study, all-cellulose ECM-mimetic cryogels were developed using binary combinations of colloidal and/or polymeric cellulose derivatives with varying aldehyde and amine functionalities. Cellulose derivatives bearing amine, aldehyde, and/or carboxylate groups are synthesized, including bifunctional HCNC (BHCNC), dialdehyde cellulose (DAC), diamine-modified HCNC (DAmHCNC), and diamine cellulose (DAmC). The HCNC and biopolymers are subsequently examined by atomic force microscopy (AFM) imaging, dynamic light scattering (DLS), or attenuated total reflection-Fourier transform infrared (ATR-FTIR) spectroscopy. The resulting cryogels are characterized through density measurements and visualization of their multiscale architecture using scanning electron microscopy (SEM). This work establishes a sustainable, all-cellulose

scaffold platform with ECM-mimetic structural features, offering potential for tissue engineering and regenerative applications.

EXPERIMENTAL

Materials

Sheets of northern bleached softwood pulp from Resolute Inc. (QC, Canada) were used as the initial material to synthesize BHCNC, DAmHCNC, DAmC, and DAC. Hydrochloric acid (HCl, ACS reagent grade, 37%), sodium chloride (NaCl, > 99.5%), sodium hydroxide (NaOH, ACS reagent grade, > 97%), sodium (meta)periodate ($NaIO_4$, > 99.0%), hydroxylamine hydrochloride ($NH_2OH{\cdot}HCl$, ReagentPlus®, 99%), sodium chlorite ($NaClO_2$, 80%), ammonium acetate ($NH_4CH_3CO_2$, ACS reagent, ≥ 97%), ammonia (NH_3) solution (2 M in ethanol), sodium borohydride ($NaBH_4$, ReagentPlus®, 99%), ethylene glycol ($C_2H_6O_2$, ReagentPlus®, > 99%), hydrogen peroxide (H_2O_2, 30 wt.%), and anhydrous isopropanol (99.5%) were purchased from MilliporeSigma, USA. Anhydrous ethanol (EtOH, 200 proof) was procured from KOPTEC Inc., USA. Dialysis membranes (molecular weight cutoff = 8 to 10 kDa) were purchased from Spectrum Laboratories Inc., TX, USA. Mica sheets (V1 grade) and AFM stainless steel disks were supplied by Ted Pella Inc. (USA) and SPI supplies (USA), respectively. Conductive double-sided adhesive carbon tape and pin stubs were procured from Rave Scientific (USA) and Oxford instruments (UK), respectively. Unless otherwise specified, ultrapure (Milli-Q) water with a resistivity of 18.2 MΩ cm at 25 °C was used for experiments. Ultrapure water was produced *via* passing deionized (DI) water through an ultrafilter (Biopak Polisher, Millipore, USA).

BHCNC Synthesis

The BHCNC were prepared according to a previously established method (Tavakolian *et al.* 2023). The softwood pulp sheets (5 g) were torn into thin pieces with dimensions of ~ 2 × 2 cm^2, and pulp fragments were soaked in 500 mL of DI water and stirred using an overhead stirrer (SH-II-6C, Faithful Instrument CO., China) for one day. Then, water was removed *via* vacuum filtration using a nylon cloth (pore size ~ 20 μm), and the wet pulp was suspended in an NaCl solution (325 mL, 1 M). Following mixing for 5 min and wrapping the beaker with aluminum foil, $NaIO_4$ (6.60 g) was added to selectively oxidize the vicinal diols of cellulose to dialdehyde groups. The reaction was mixed at ambient temperature for 42 h. To stop the reaction, 5 mL of ethylene glycol was incorporated and stirred for 10 min to deactivate unreacted $NaIO_4$. The oxidized pulp, referred to as dialdehyde-modified cellulose (DAMC), were then vacuum filtered and rinsed with DI water at least 5 times (250 mL each time) to remove residual chemicals and byproducts.

To convert about half of the DAMC aldehyde groups to carboxylate groups and isolate BHCNC, DAMC was further oxidized with $NaClO_2$. To this end, DAMC fibrils were suspended in DI water (250 mL, including the water in the wet DAMC), followed by the addition of $NaClO_2$ (4.22 g) and NaCl (14.12 g). Then, H_2O_2 (4.22 g) was added dropwise within ~ 30 s and stirred at 100 rpm for 12 h. The pH was adjusted to ~ 5.0 ± 0.2 using an NaOH solution (0.5 M) during the reaction. The bifunctional fibrils were separated *via* centrifugation at 8000 × ***g*** for 10 min and rinsed with an ethanol solution in DI water (70 v/v%, 100 mL) for at least three times. The fibrils were suspended in DI water (500

mL) and heated at 80 °C for 2 h, then centrifuged at 8000 × *g* for 20 min to separate the unfibrillated cellulose. The BHCNC particles in the supernatant were precipitated by adding a nonsolvent (ethanol, volume ~ 1.5 times the supernatant volume), collected by centrifugation at 8000 × *g* for 20 min, and purified by dialysis (Spectra/Por membranes, molecular weight cutoff = 8 to 10 kDa) against DI water for one day. The conductivity of dialysate solution (water surrounding the dialysis bags) was periodically measured using a conductivity meter (VWR sympHony B40PCID, USA) until it approached that of pure DI water, indicating complete purification. The BHCNC concentration was increased to ~ 4 wt% *via* evaporation at 40 °C under constant airflow for further use. The concentration was measured by oven-drying a known volume of BHCNC dispersion at 70 °C, followed by weighing.

DAC Synthesis

To synthesize fully solubilized DAC, a previously established protocol was followed (Yang *et al.* 2015). The softwood pulp sheets (10 g) were torn into thin pieces with dimensions of ~ 2 × 2 cm^2, and pulp fragments were soaked in 1 L of DI water and stirred using an overhead stirrer (SH-II-6C, Faithful Instrument CO., China) for one day. Then, water was removed by vacuum filtration using a nylon cloth (pore size ~ 20 μm), and the wet pulp with 38 g of NaCl was added to 650 mL of DI water. Following mixing for 5 min and wrapping the beaker with aluminum foil, $NaIO_4$ (13.2 g) was added and dissolved. The mixture was then stirred at ambient temperature for 6 days to maximize the oxidation of hydroxyl groups. To stop the reaction, 10 mL of ethylene glycol was added and mixed for 15 min, deactivating unreacted $NaIO_4$. Finally, in 500 mL of ultrapure water, DAC fibrils were dispersed and heated at 60 °C for 8 h to obtain solubilized DAC, and the unfibrillated cellulose was separated by centrifugation at 8000 × *g* for 20 min. The DAC concentration was increased to ~ 10 wt% *via* evaporation at 40 °C under constant airflow for further use.

DAmHCNC and DAmC Synthesis

To synthesize diamine-functionalized cellulose derivatives, the authors' previously established method was followed (Koshani *et al.* 2022). DAMC fibrils were prepared following the protocol in the "BHCNC Synthesis" section and dehydrated by mixing the wet fibers in 200 proof ethanol for 3 cycles to exchange the solvents. Cycles included dispersing the DAMC in ethanol for 10 h, followed by centrifugation 8000 × *g* for 5 min. The solvent-exchanged DAMC (4 g) with 5.5 mmol g^{-1} –CHO was then dispersed in ethanol (200 mL) to which 1.7 g of $NH_4CH_3CO_2$ (3 mol for each mol of –CHO) and 55 mmol of NH_3 per gram of DAMC (10 mol for each mol of –CHO) were added. The suspension was mixed at 80 °C and refluxed for 18 h, then cooled using an ice bath, and 0.46 g of $NaBH_4$ was slowly introduced into the mixture. After 1 h of stirring, diamine-functionalized fibrils were washed at least 5 times with DI water. A portion of the resulting fibrils (2 g) was added to 100 mL of DI water with pH adjusted to ~ 2.5 using an HCl solution (0.1 M) to protonate the amine groups, and the mixture was stirred for 15 min to disperse. The suspension was heated to 60 °C in an oil bath and stirred for 1.5 h, followed by centrifugation at 8000 × *g* for 15 min to separate unfibrillated fibrils. DAmHCNC was precipitated from the supernatant by adding isopropanol (~ 1.5 times the supernatant weight) and collected by centrifugation at 8000 × *g* for 15 min. Further isopropanol was added to precipitate the DAmC in the remaining supernatant. The precipitated DAmHCNC particles and DAmC were redispersed in 10 mL of ultrapure water and purified via dialysis

(Spectra/Por membranes, molecular weight cutoff = 8 to 10 kDa) against ultrapure water for one day. The conductivity of the dialysate was measured until it approached that of ultrapure water. The concentration of aminated cellulose derivatives was increased to ~ 1 wt% *via* evaporation at 40 °C under constant airflow for further use.

Functional Group Measurement

The aldehyde group content of DAMC and DAC was measured following literature (Kim *et al.* 2000a). Never-dried DAMC (30 mg, based on dry mass) or DAC (25 mg, based on dry mass) was added to 50 mL of ultrapure water. The suspension pH was then adjusted to 3.5 using HCl (0.1 M). Subsequently, 10 mL of 5 wt.% $NH_2OH{\cdot}HCl$ solution, with a pre-adjusted pH to 3.5 using HCl (0.1 M), was added to the suspension. The reaction of $NH_2OH{\cdot}HCl$ with DAMC or DAC dialdehyde groups led to the release of HCl, decreasing pH to < 3.5. The aldehyde group content was quantified by titrating the mixture with a NaOH solution (10 mM) at 0.1 mL min^{-1} using an automated titrator (Metrohm 907 Titrando, USA) until the pH stabilized at 3.5.

Conductometric titration was conducted to measure the content of BHCNC carboxylate groups. The never-dried BHCNC (45 mg, based on dry mass) was dispersed in 140 mL of ultrapure water. Subsequently, the dispersion pH was adjusted to 3 using an HCl solution (0.1 M). The titration proceeded with a NaOH solution (10 mM) at a rate of 0.1 mL min^{-1} using an automated titrator (Metrohm 907 Titrando, USA) until pH reached ~ 11. The carboxylate group content was determined by measuring the volume of NaOH consumed to neutralize the carboxylate groups (*i.e.*, weak acid groups) (Araki *et al.* 2001).

The primary amine group content of DAmHCNC or DAmC was determined following the authors' previously reported protocol (Koshani *et al.* 2022). The never-dried materials (20 mg, based on dry mass) were dispersed in 140 mL of ultrapure water, and the pH was adjusted to ~ 11.5 with a NaOH solution (0.1 M). The titration proceeded with an HCl solution (5 mM) at 0.1 mL min^{-1} using an automated titrator (Metrohm 907 Titrando, USA) until pH ~ 3. The amine content was determined from the plateaued region of titration curve, representing the HCl solution volume required to neutralize the weak base (i.e., amine groups).

Hydrodynamic Size and ζ-Potential Measurements

To determine the hydrodynamic equivalent size of colloidal and polymeric cellulose derivatives, a Zetasizer Nano series instrument (Malvern Inc., UK) at a scattering angle of 90° was used at 25 °C. The sample concentration was adjusted to 0.1% w/v using ultrapure water, followed by pipetting 70 µL into a low-volume quartz cuvette (ZEN2112, Malvern, UK). The *Z*-average values (cumulants mean) were reported as the hydrodynamic equivalent size.

To determine the ζ-potential, the electrophoretic mobility of samples was measured using the Zetasizer Nano series instrument (Malvern Inc., UK) at 25 °C and pH = 5.7. Before conducting the measurements, samples were diluted to 0.1% w/v using ultrapure water, followed by pipetting a desired volume (900 µL) into disposable folded capillary cells (Malvern, UK). To apply the effect of BHCNC and DAmHCNC rod-like geometry to the ζ-potential value, Ohshima's mobility expression was used (Ohshima 1996). Since κa < 1 (κ is the Debye-Hückel parameter, and a is the nanoparticle diameter, obtained from the AFM image analysis), the Henry's function $f(\kappa a) \sim 0.5$, and equation 1 was used to estimate the ζ-potential using the electrophoretic mobility,

$$\mu_{av} = \frac{\mu_{\parallel} + 2\mu_{\perp}}{3} = \frac{\varepsilon_r \varepsilon_0}{3\eta} \zeta [1 + 2f(\kappa a)] \quad (1)$$

where $\mu_{\parallel}$ and $\mu_{\perp}$ are the electrophoretic mobility of rod-like particles in the parallel and perpendicular direction to the electric field, respectively, ε_r is the relative dielectric permittivity of solvent, ε_0 is the dielectric permittivity in a vacuum (vacuum permittivity), and η is the electrolyte viscosity. The ionic strength was calculated by considering the counterions (Na^+ or H^+) of BHCNC carboxylate groups or DAmHCNC amine groups. For the biopolymers (DAC and DAmC), the ζ-potential was obtained using the Smoluchowski equation.

ATR-FTIR Spectroscopy

The characteristic chemical bonds of cellulose derivatives were identified using an FTIR spectrometer (Fisher Scientific, USA). A single-reflection diamond ATR crystal was used for the spectrometer. Samples were first frozen at -80 °C, followed by sublimating the ice at 0.01 mbar overnight using a FreeZone benchtop freeze dryer (Labconco, USA). The dried materials were directly placed onto the ATR crystal, and the maximum pressure was applied by lowering the pressure clamp with an incident angle of 45°. Spectra were collected by averaging 100 scans with a wavenumber range of 4000 to 500 cm^{-1} at 6 cm^{-1} resolution. The clean bare diamond surface was measured and subtracted as background for each sample scanned.

AFM Imaging

To investigate DAmHCNC and BHCNC morphology, an atomic force microscope (Bruker Dimension Icon I, USA), equipped with a silicon nitride probe (Bruker ScanAsyst-Air, USA) was used in the PeakForce tapping mode. A droplet (~10 µL) of each dispersion (concentration ~ 0.1 mg mL^{-1}) was separately deposited on a freshly cleaved mica sheet, secured to a magnetic stainless-steel disc. After air-drying overnight at ambient temperature, the discs were washed with ultrapure water five times (200 µL each time) and completely dried at room temperature before imaging. The AFM images were analyzed using the NanoScope Analysis (version 1.80, accessed through Penn State MCL), followed by measuring the diameter (*i.e.*, height) of ~ 50 nanoparticles (n = 1).

Cryogel Preparation

Biomimetic hydrogels were formed *via* (i) dynamic covalent crosslinking of DAC with DAmHCNC or DAmC; or (ii) physical (electrostatic) and dynamic covalent crosslinking of BHCNC with DAmHCNC or DAmC at varying mass ratios. The following hydrogels (~ 10.5 mL) were first prepared.

(i) BHCNC-DAmHCNC: The BHCNC (4 wt%, 1 mL) dispersion was mixed with ~ 8.5 mL, ~ 2.9 mL, or ~ 1 mL of DAmHCNC (1 wt%) to obtain a -CHO:-NH_2 molar ratio of ~ 1:3, ~ 1:1, or ~ 3:1, respectively, followed by adding ultrapure water to reach ~ 10.5 mL.

(ii) BHCNC-DAmC: The BHCNC (4 wt%, 1 mL) dispersion was mixed with ~ 9.6 mL, ~ 3.2 mL, or ~ 1.1 mL of DAmC (1 wt%) to obtain a -CHO:-NH_2 molar ratio of ~ 1:3, ~ 1:1, or ~ 3:1, respectively, followed by adding ultrapure water to reach ~ 10.5 mL.

(iii) DAC-DAmHCNC: The DAC (10 wt%, 0.15 mL) dispersion was mixed with ~ 9.1 mL, ~ 3.1 mL, or ~ 1 mL of DAmHCNC (1 wt%) to obtain a -CHO:-NH_2 molar ratio of ~ 1:3, ~ 1:1, or ~ 3:1, respectively, followed by adding ultrapure water to reach ~ 10.5 mL.

(iv) DAC-DAmC: The DAC (10 wt%, 0.15 mL) dispersion was mixed with ~ 10.2 mL, ~ 3.4 mL, or ~ 1.1 mL of DAmC (1 wt%) to obtain a -CHO:-NH_2 molar ratio of 1:3, 1:1, or 3:1, respectively, followed by adding ultrapure water to reach ~ 10.5 mL.

The mixtures were mixed using a positive displacement pipette (Microman E M1000E, Gilson, OH, USA) for ~ 30 s and incubated at 60 °C for 1 h to form hydrogels. To convert the hydrogels to cryogels, samples were frozen at -80 °C in a freezer for ~ 12 h, followed by sublimating the ice at 0.01 mbar overnight using a FreeZone benchtop freeze dryer (Labconco, USA).

SEM Imaging

Cryogels were secured to specimen stubs with a double-sided carbon tape and sputter-coated with a 3 nm-thick indium layer using a vacuum sputtering instrument (Leica sputter coating EM ACE 600, USA). The samples were then imaged using SEM (Thermo Scientific Verios G4, USA) with an accelerating voltage of 5 to 10 kV and a beam current of 0.1 to 14 nA.

Density Measurement

To measure cryogel density, cylindrical samples were prepared and weighed. The cylinder dimensions were then measured with a digital caliper, and the volume was calculated. Finally, the density was determined by dividing the cryogel weight (g) by the volume (cm^3) (Chen *et al.* 2021).

Statistical Analyses

The data are presented as the average of three independent samples (n = 3) ± standard deviation (SD) values. Statistical significance was determined using Student's *t*-test for comparisons among two groups (Figures 3C-3F), and one-way analysis of variance (ANOVA), followed by the Tukey's post-hoc test for comparisons among three or more distinct groups (Fig. 5A). The p-values of $p < 0.05$ were considered significant, corresponding to the symbols *, **, ***, and **** for $p < 0.05$, $p < 0.01$, $p < 0.001$, and $p < 0.0001$, respectively. The p-values of $p \geq 0.05$ were considered nonsignificant (ns). Statistical analyses were performed using GraphPad Prism (version 9.4.1, USA).

RESULTS AND DISCUSSION

Development of Colloidal and Polymeric Cellulose

The building blocks of cryogels in this study were BHCNC (CNC with aldehyde- and carboxylate-bearing disordered cellulose chains), DAC (fully solubilized, aldehyde-bearing disordered cellulose polymers), DAmHCNC (CNC with amine-bearing disordered cellulose chains), and DAmC (fully solubilized, amine-bearing disordered cellulose polymers), as shown in Fig. 1. DAMC fibrils with partially aldehyde group-modified C2 and C3 are synthesized *via* a 42-h periodate reaction of cellulose fibrils, as presented in Fig. 1A, and used as an intermediate precursor for cellulose derivatives, except for DAC. Periodate stereospecifically oxidizes the C2-C3 vicinal diols to dialdehyde groups and simultaneously cleaves the C2-C3 bond (Kim *et al.* 2000b; van de Ven and Sheikhi 2016).

Figure 1B shows BHCNC synthesis through the 12-h chlorite oxidation of DAMC fibrils by which a fraction of aldehyde groups is converted to carboxylate groups, followed

by the heating (2 h) of bifunctional fibrils at 80 °C, yielding BHCNC and solubilized cellulose.

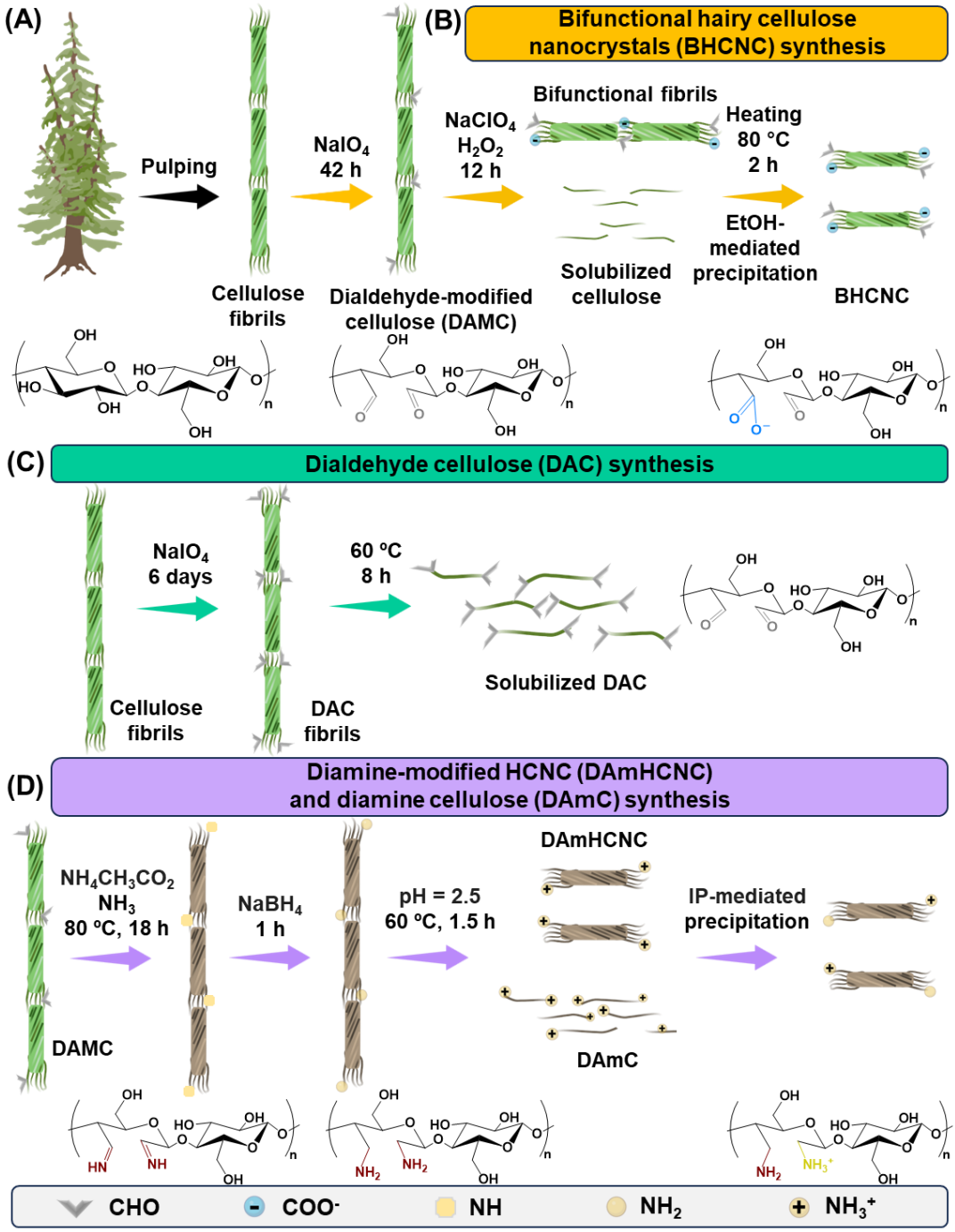


Fig. 1. Synthesis and characterization of colloidal and polymeric cellulose derivatives. Schematic of **(A)** DAMC fibril synthesis *via* the periodate oxidation of cellulose fibrils, used for **(B)** BHCNC preparation *via* the partial chlorite oxidation of fibrils, followed by heating and ethanol-mediated isolation. **(C)** DAC preparation *via* the periodate oxidation of cellulose fibrils, followed by heating. **(D)** DAmHCNC or DAmC preparation *via* the reductive amination of DAMC fibrils, followed by pH-mediated amine protonation, heating, and isopropanol-mediated isolation. The corresponding changes in cellulose chemical structure during the chemical reactions are shown in all panels.

Non-solvent (ethanol)-mediated fractional precipitation is conducted to separate BHCNC from solubilized cellulose. Figure 1C presents DAC synthesis through the 6-day periodate oxidation of cellulose fibrils, maximizing conversion of C2-C3 hydroxyl groups to aldehyde groups and the cleavage of C2-C3 bond. As shown in Fig. 1D, *via* leveraging the reactive aldehyde groups of DAMC fibrils, amine-bearing cellulose derivatives were synthesized through the reductive amination reaction of fibrils, followed by adjusting pH to 2.5 to protonate amine groups and heating at 60 °C, resulting in a dispersion of mixed DAmHCNC and DAmC. A Schiff base reaction involving DAMC aldehyde groups and ammonia yields imine bonds, which are reduced to primary amine groups using sodium borohydride as a reducing agent. Non-solvent (isopropanol, IP)-mediated fractional precipitation is conducted to separate DAmHCNC from DAmC.

Functional Groups Content of Colloidal and Polymeric Cellulose Derivatives

The pH titration curves of DAMC fibrils and solubilized DAC are shown in Figs. 2A and 2B, respectively, indicating the amount of NaOH (10 mM) required to neutralize the HCl released from the hydroxylamine-aldehyde reaction. Accordingly, the aldehyde content of DAMC, as a precursor for BHCNC and DAmHCNC synthesis, was ~ 5.5 ± 0.3 mmol g^{-1}, and for DAC it was ~ 9.1 ± 1.2 mmol g^{-1}. The degree of substitution (DS) takes the average of hydroxyl groups per anhydroglucose unit that are converted to final groups. Full oxidation led to the transformation of two out of three hydroxyl groups in each unit and thus a DS of 2, corresponding to an aldehyde group content of 12.6 mmol g^{-1}. Therefore, the DS of DAC was ~ 1.4.

Figure 2C presents the conductometric titration curve, obtained to measure the carboxylate group content of BHCNC. The BHCNC carboxylate group content was ~ 2.3 ± 0.7 mmol g^{-1}, which was calculated from the NaOH (10 mM) volume required to neutralize the carboxylic acid (*i.e.*, weak acid). The content of BHCNC aldehyde groups (~ 3.2 mmol g^{-1}) was then estimated by subtracting the introduced carboxylates to BHCNC from the total aldehyde groups of DAMC (Fig. 2A). The amine content of DAmHCNC and DAmC was 4.5 ± 0.2 and ~ 4.0 ± 1.6 mmol g^{-1}, respectively, which is based on the amount of HCl necessary to neutralize the weak base ($R{-}NH_2 + HCl \rightarrow R{-}NH^{3+} + Cl^-$), as shown in Figs. 2D and 2E, respectively.

Characterization of Colloidal and Polymeric Cellulose Derivatives

The morphology and dimensions of hairy nanocelluloses were examined using AFM imaging. Figures 3A and 3B show representative AFM images of DAmHCNC and BHCNC, respectively. Both nanocelluloses had a rod- or needle-like morphology, which is consistent with those of previous HCNC, isolated *via* periodate/chlorite oxidation reactions (Yang *et al.* 2016) or oxidation/reductive amination reactions (Koshani *et al.* 2022). Notably, the positively charged DAmHCNC readily adsorbed negatively charged impurities present in water, leading to particle aggregation that was also observed in the AFM image. The diameter (*i.e.*, height) of DAmHCNC and BHCNC were 5 ± 3 nm and 4 ± 2 nm, respectively, as determined from the AFM images of ~ 50 individual particles (n = 1). The apparent width of particles in AFM images does not represent the real diameter of nanocrystals due to the tip adhesion effect in overlapping particles. Diameter is instead obtained from the height difference between the top of nanocrystals and the underlying mica substrate.

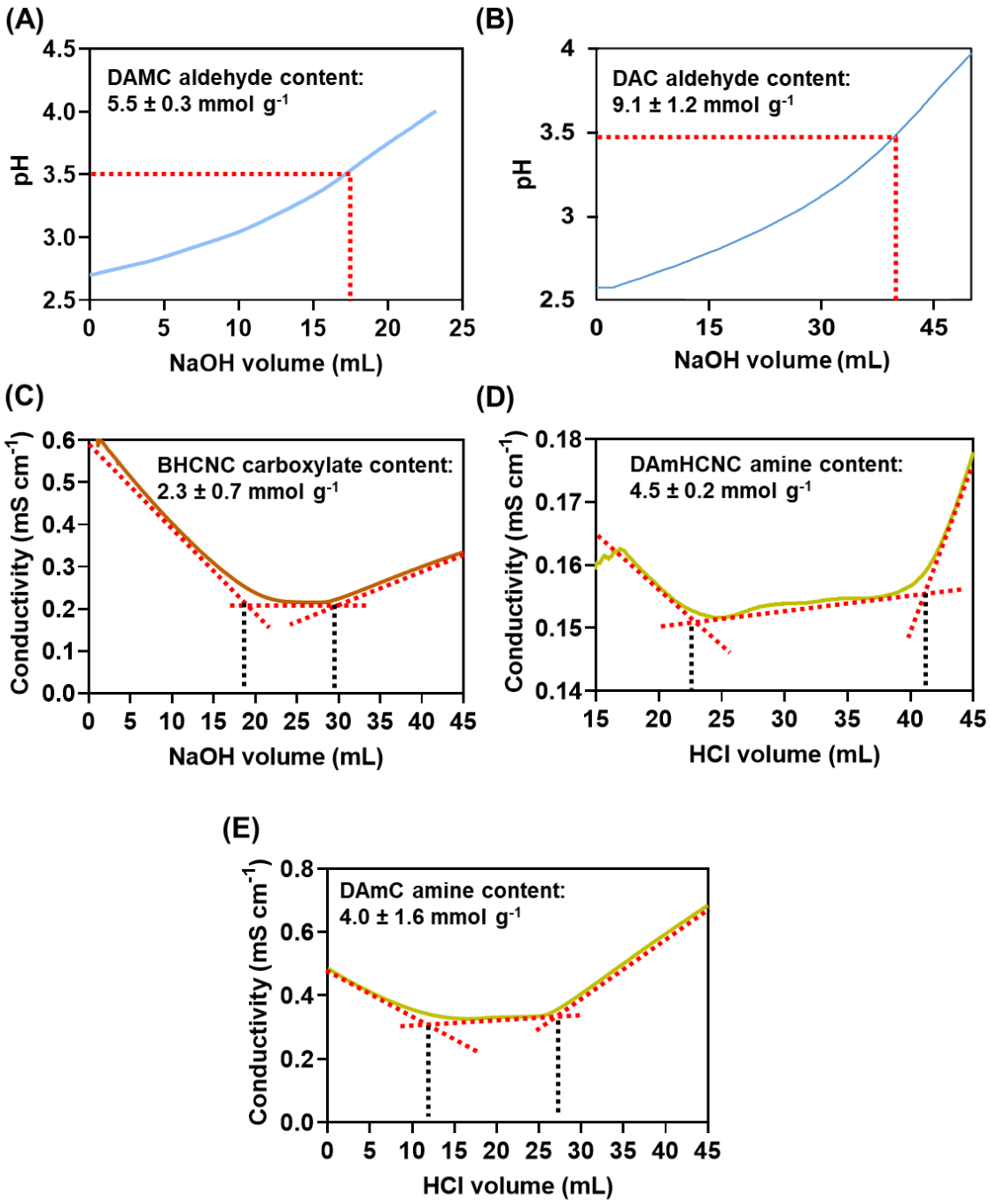


Fig. 2. Functional group content of colloidal and polymeric cellulose derivatives: Representative pH titration curves of **(A)** DAMC and **(B)** DAC for measuring the aldehyde group content. Representative conductometric titration curves of **(C)** BHCNC for measuring the carboxylate groups using a strong base (10 mM NaOH), and **(D)** DAmHCNC and **(E)** DAmC for measuring the amine groups using a strong acid (5 mM HCl).

Figures 3C and 3D show the hydrodynamic equivalent size of aldehyde-bearing (BHCNC and DAC) and amine-bearing (DAmHCNC and DAmC) cellulose derivatives, respectively.

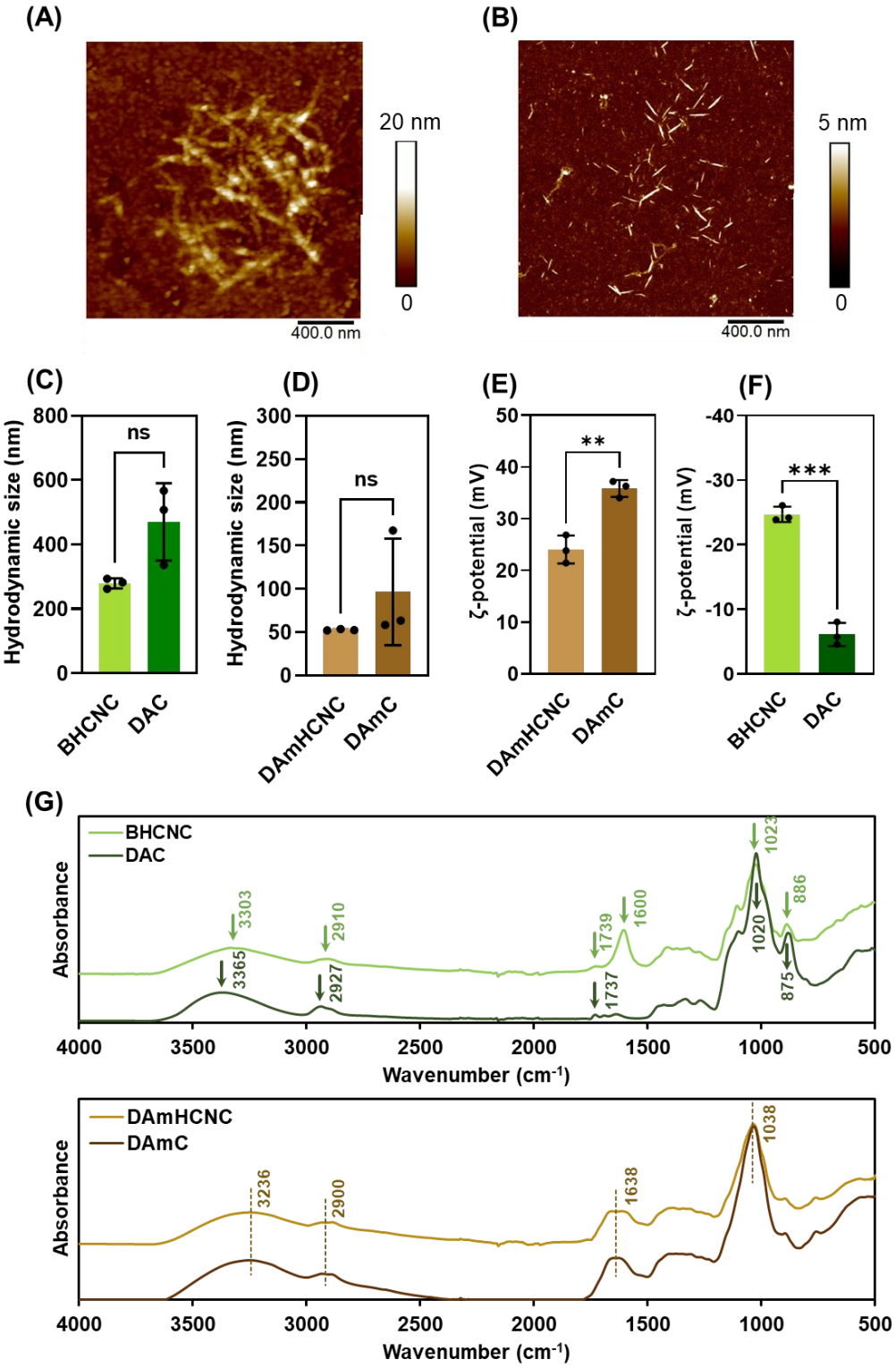


Fig. 3. Characterization of colloidal and polymeric cellulose derivatives. AFM images of **(A)** DAmHCNC and **(B)** BHCNC, showing their rod-like morphology. Hydrodynamic size of **(C)** BHCNC and DAC, and **(D)** DAmHCNC and DAmC. ζ-potential of **(E)** DAmHCNC (ionic strength ~ 4 mM) and DAmC (ionic strength ~ 4.5 mM) at pH ~ 5.7, and **(F)** BHCNC (ionic strength ~ 2.3 mM) and DAC at pH ~ 5.7. **(G)** ATR-FTIR spectra of BHCNC and DAC, indicating characteristic aldehyde groups, and of DAmHCNC and DAmC, confirming characteristic amine groups. ns $p \geq 0.05$, ** $p < 0.01$, and *** $p < 0.001$.

The hydrodynamic size (equivalent diameter) of BHCNC and DAC was ~ 279 ± 16 nm and 470 ± 120 nm, respectively, while that of DAmHCNC and DAmC was ~ 53 ± 1 nm and 96 ± 61 nm, respectively. The smaller hydrodynamic size of DAmC and DAmHCNC compared with aldehyde-bearing derivatives may originate from the acidic treatment at a higher temperature during the synthesis, leading to the more extensive dissolution and fragmentation of cellulose chains.

Figure 3E presents the DAmHCNC and DAmC ζ-potential, which was ~ +24 ± 3 mV (ionic strength ~ 4.5 mM) and ~ +36 ± 2 mV (ionic strength ~ 4 mM) at pH ~ 5.7, respectively, confirming the positively charged amine groups on the nanocellulose and polymer. Figure 3F shows the ζ-potential values of BHCNC (ionic strength ~ 2.3 mM) and DAC at pH ~ 5.7. The BHCNC and DAC ζ-potential were ~ -25 ± 1 and ~ -6 ± 2 mV, respectively, confirming their negatively charged surfaces. DAC is expected to be electrically neutral; however, negatively charged impurities in solution may adsorb to it, resulting in a negative ζ-potential, which has been reported in the literature (Chen and van de Ven 2016).

To examine the successful functionalization of colloidal and polymeric cellulose derivatives, ATR-FTIR spectra were obtained. Figure 3G presents the ATR-FTIR spectra of BHCNC, DAC, DAmHCNC, and DAmC. In the spectra of all cellulose derivatives, characteristic peaks of cellulose were at ~ 3700 to 3000 cm^{-1}, ~ 2950 to 2900 cm^{-1}, and ~ 1050 to 1000 cm^{-1}, corresponding to O–H, C–H, and CH_2–O–CH_2 stretching vibrations, respectively (Hishikawa *et al.* 2017; Kondo and Sawatari 1996; Koshani *et al.* 2024). In DAC and BHCNC spectra, peaks at ~ 1737 and ~ 1739 cm^{-1} correspond to the stretching vibrations of carbonyl groups (C=O), which were due to aldehyde formation after periodate oxidation. The increased intensity of the peaks at ~ 886 and ~ 875 cm^{-1} compared with intact cellulose has been attributed to the interactions between aldehyde groups and neighboring hydroxyl groups, resulting in a hemiacetal linkage (Kim *et al.* 2000a; Koshani *et al.* 2025). The BHCNC spectrum showed a peak at ~ 1600 cm^{-1}, representing the C=O stretching vibration of carboxylate groups. In the spectra of DAmHCNC and DAmC, a peak at ~ 1638 cm^{-1} corresponds to the C–NH_2 bending vibrations. It is also noted that the absorption peaks related to amine groups, which reside in the range of ~ 3400-3250 cm^{-1}, overlap with the O-H stretching vibrations in cellulose (Koshani *et al.* 2022; OpenStax 2016). Together, the FTIR spectra verify the successful functionalization of cellulose derivatives with reactive aldehyde and amine groups.

All-Cellulose Cryogels with ECM-Mimetic Architecture

The design strategy and fabrication pathway for ECM-mimetic all-cellulose cryogels, constructed from chemically-functionalized colloidal and polymeric cellulose derivatives, are shown in Fig. 4. The cryogel engineering integrates aldehyde-bearing cellulose derivatives (DAC or BHCNC) with amine-bearing counterparts (DAmC or DAmHCNC), enabling controlled assembly *via* a combination of dynamic covalent bonding and physical interactions (Fig. 4A). Upon mixing, aldehyde and primary amine groups undergo a Schiff base reaction, forming imine crosslinks that establish dynamic hydrogel networks. Electrostatic interactions between oppositely charged DAmHCNC or DAmC cellulose derivatives with negatively charged BHCNC may further contribute to network formation. The binary assembly approach allows nanoparticles (BHCNC or DAmHCNC) and polymers (DAC or DAmC) to participate synergistically in network formation, leading to hierarchical structures across multiple length scales. As presented in

Fig. 4B, the lyophilization of hydrogels yields freestanding cryogels with highly porous architectures. Images of representative cryogels are presented in Fig. A1 (Appendix). As shown schematically, this process translates physicochemical interactions, such as hydrogen bonding, electrostatic attraction, dynamic imine bond formation, and colloidal assembly, into scaffolds with unique pore features.

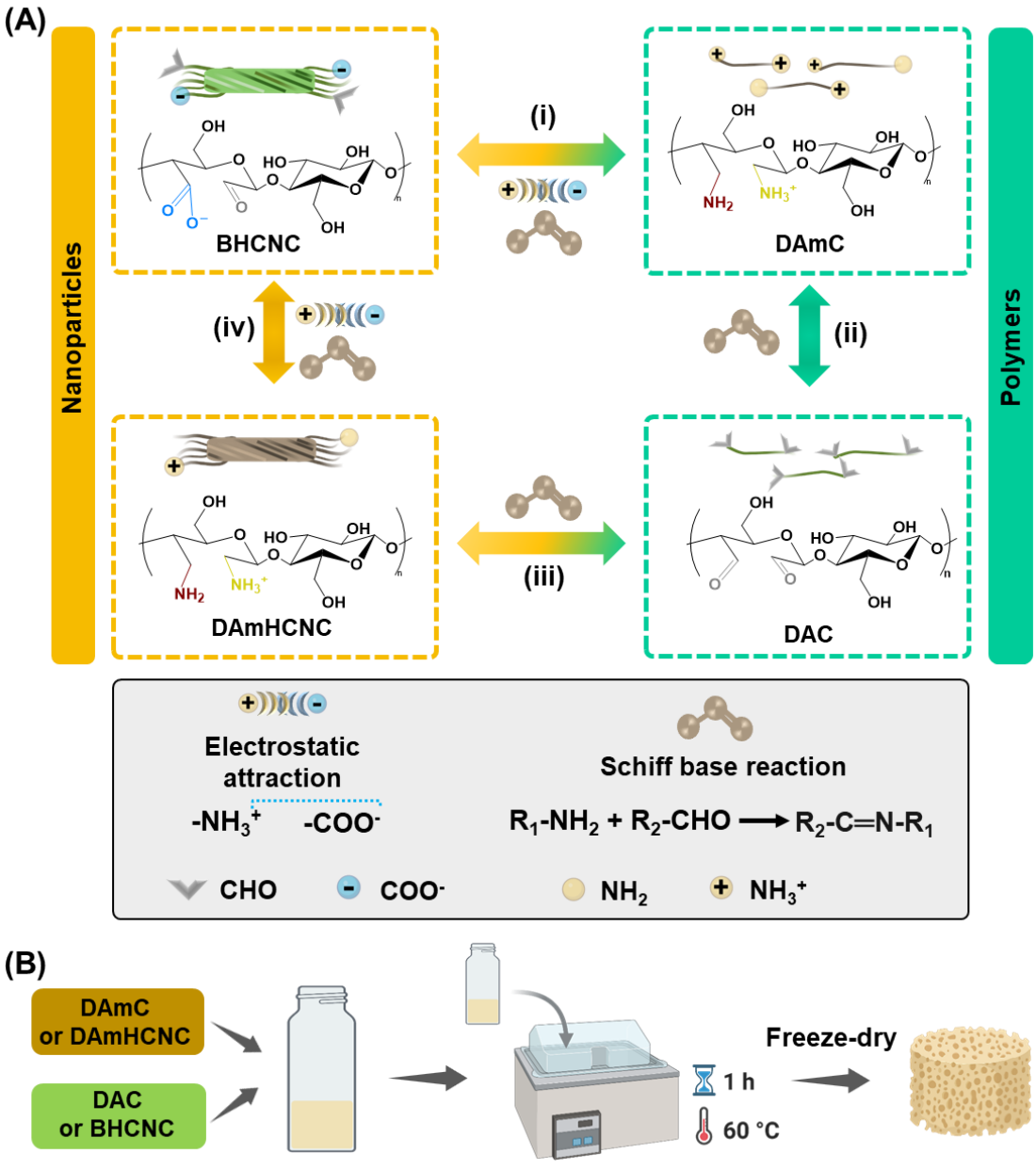


Fig. 4. Design of ECM-mimetic all-cellulose cryogels. **(A)** Building blocks for the design of cryogels, including nanoparticles (BHCNC or DAmHCNC) and biopolymers (DAC or DAmC), along with the corresponding physicochemical interactions, including electrostatic attraction and/or Schiff base reaction. Aldehyde-bearing BHCNC or DAC are independently mixed with amine-bearing DAmHCNC or DAmC at varying aldehyde to amine molar ratios. **(B)** Cryogel fabrication by mixing aldehyde-bearing DAC or BHCNC with amine-bearing DAmC or DAmHCNC, followed by heating at 60 °C for 1 h and subsequent freeze-drying.

Characterization of Cryogels

Figure 5 presents the density measurements and the structure of all-cellulose cryogels, formed *via* polymer-polymer, nanoparticle-polymer, and nanoparticle-nanoparticle interactions at varying –CHO:–NH_2 molar ratios. A representative image of cryogels incubated in ultrapure water for three months is shown in Fig. A2 (Appendix), indicating the long-term structural stability of cryogels.

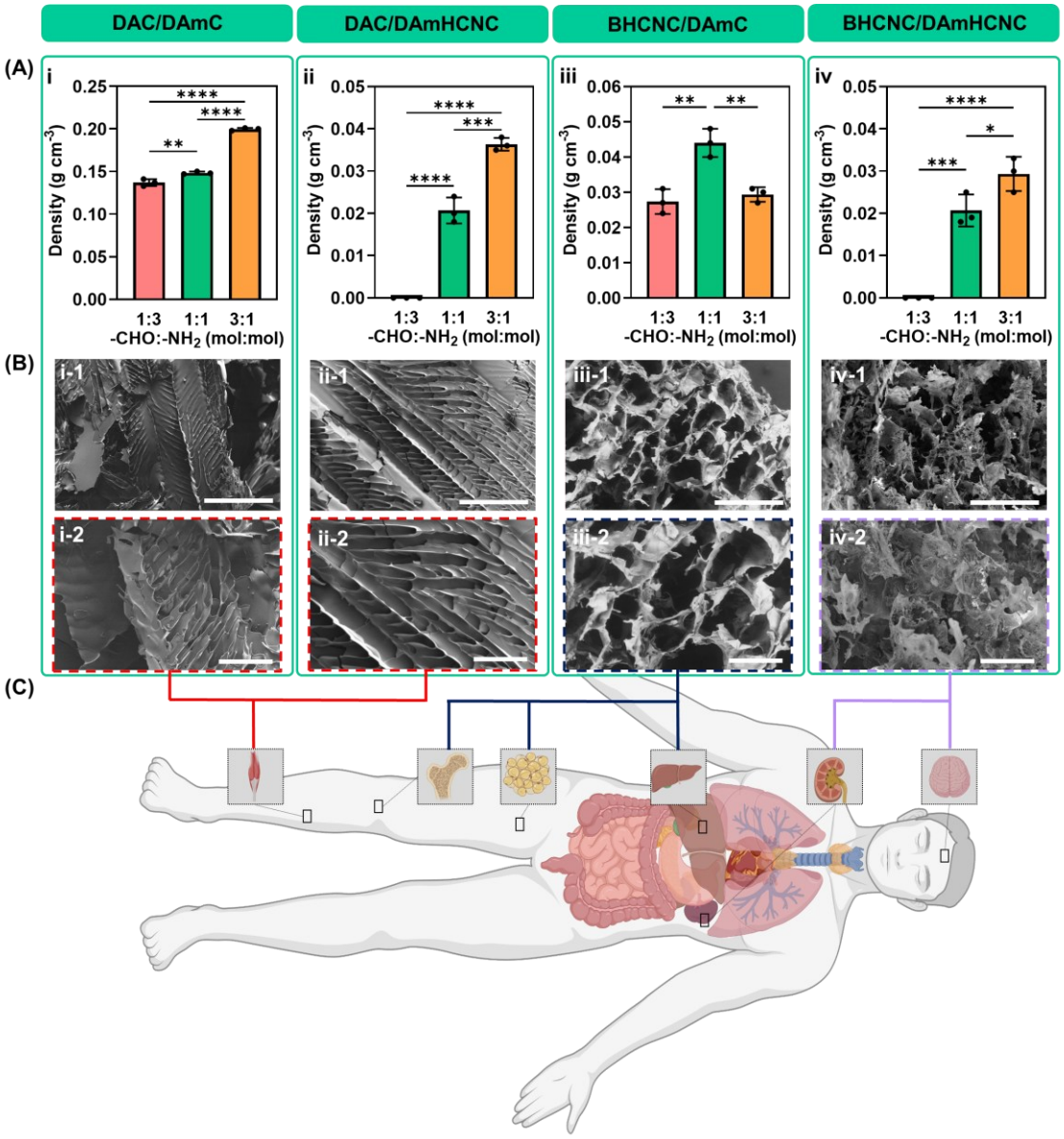


Fig. 5. Density and morphological assessments of ECM-mimetic all-cellulose cryogels. **(A)** Density values of (i) DAC/DAmC, (ii) DAC/DAmHCNC, (iii) BHCNC/DAmC, and (iv) BHCNC/DAmHCNC cryogels, resulting from polymer-polymer, polymer-nanoparticle, and nanoparticle-nanoparticle interactions at varying –CHO:–NH_2 molar ratios along with **(B)** the SEM images of corresponding cryogels at a constant 1:1 –CHO:–NH_2 molar ratio. **(C)** Schematic relating the biomimetic cryogel structures to native ECM in different tissues, including muscle, bone, adipose, liver, kidney, and brain. **** $p < 0.0001$, *** $p < 0.001$, ** $p < 0.01$, and * $p < 0.05$. Non-significant $p \geq 0.05$ is not shown. Scale bars in i-1, ii-1, iii-1, and iv-1 images are 500 µm. Scale bars in i-2, ii-2, iii-2, and iv-2 images are 200 µm.

Figure 5A(i-iv) presents the density values of cryogels. Polymer-polymer cryogels (DAC/DAmC) exhibited the highest density, likely resulting from the extensive chain packing and limited pore expansion during freeze-drying. In comparison, polymer-nanoparticle or nanoparticle-nanoparticle scaffolds (DAC/DAmHCNC, BHCNC/DAmHCNC, and BHCNC/DAmC) had significantly lower densities. Nanoscale BHCNC and DAmHCNC may disrupt the polymer chain packing, leading to a lower density. Except for BHCNC/DAmC, cryogel density increased as the aldehyde-to-amine molar ratio increased. The lower density of nanoparticles-containing cryogels compared with the polymer-polymer (DAC/DAmC) counterpart may be attributed to the "hairy" domains attached to nanocrystals, leading to a percolated, open network with increased pore volume and, consequently, lower overall density.

SEM imaging was conducted to elucidate the microstructure of all-cellulose cryogels, fabricated at a 1:1 –CHO:–NH_2 molar ratio, as shown in Fig. 5B. Across all compositions, pronounced differences in pore morphology were observed depending on whether the network was formed using polymeric cellulose derivatives, hairy nanocelluloses, or combinations thereof. DAC/DAmC and DAC/DAmHCNC cryogels showed relatively dense lamellar structures with aligned, sheet-like walls and qualitatively lower void fraction, which may mimic the ECM of muscle and tendon tissues (Fig. 5C). This morphology is consistent with strong chain packing and restricted network formation during freezing-induced ice crystal growth, leading to elongated, anisotropic pores. The BHCNC/DAmHCNC and BHCNC/DAmC cryogels exhibited more heterogeneous and open porous networks. The BHCNC incorporation likely promoted branching and junction formation, resulting in a more isotropic microstructure with larger and more irregular pores. The BHCNC/DAmC cryogels exhibited architectures resembling the ECM of bone and kidney tissues, whereas BHCNC/DAmHCNC cryogels more closely mimic the ECM of liver and adipose tissues (Fig. 5C). Additional images pertaining to the all-cellulose cryogels fabricated at a 3:1 –CHO:–NH_2 molar ratio are shown in Fig. A3 (Appendix).

Together, these results indicate the feasibility of engineering all-cellulose ECM-mimetic scaffolds in which low density, high porosity, and interconnected microstructures are critical for cell infiltration and regenerative performance, which warrant further investigation. Future studies may focus on establishing structure-property-function relationships and further validating the regenerative potential of these scaffolds.

CONCLUSIONS

1. In this work, fully bio-based cryogels with extracellular matrix (ECM)-mimetic architectures were engineered through the chemical functionalization and physico-chemical assembly of cellulose derivatives.
2. By leveraging aldehyde- and amine-functionalized colloidal and polymeric cellulose derivatives, a versatile strategy was developed that enables the formation of dynamic hydrogel networks *via* reversible Schiff base chemistry and physical interactions. Subsequent freeze-drying effectively translated nanoscale organization into macroscopic, porous cryogels with tunable density, pore morphology, and structural anisotropy.

3. Comparing the polymer-polymer, nanoparticle-polymer, and nanoparticle-nanoparticle assemblies indicated the critical role of hairy cellulose nanocrystals (HCNC) in the network formation and overall scaffold pore architecture.
4. Cryogels containing bifunctional hairy cellulose nanocrystals (BHCNC) and diamine-modified hairy cellulose nanocrystals (DAmHCNC) had lower density and highly porous microstructures. The resulting cryogels had architectures that mimic the ECM of varying native tissues, including muscle, bone, kidney, liver, adipose, and brain tissue, highlighting the tunability and biomimetic potential of this platform.
5. This work may pave the way for developing a sustainable and structurally programmable class of biomaterials for a broad range of applications, including *in vitro* ECM models, tissue engineering, and soft robotics.

ACKNOWLEDGEMENTS

A. Sheikhi acknowledges the support of Dorothy Foehr Huck and J. Lloyd Huck Early Career Chair. K. Akelaitis and A. Sheikhi would like to thank the Penn State College of Engineering Summer Research Experiences for Undergraduates (REU) program, which was supported by the National Science Foundation (EEC-1950639). We would like to acknowledge Dr. A. Zydney for use of the DLS instrument. Parts of Figs. 1, 4, and 5 were created with BioRender.com.

Conflict of Interest

Authors do not have any personal interest or relationship that could potentially be affected by the publication of this manuscript.

REFERENCES CITED

Amini, M., Isari, A. A., Ghasemi, S., Banvillet, G., Rojas, O. J., Kamkar, M., and Arjmand, M. (2025). "Tailoring pore structure in nanocellulose cryogels: Enhancing thermal and electromagnetic interference shielding properties," *Carbohydrate Polymers* 357, article 123435. https://doi.org/10.1016/j.carbpol.2025.123435

Araki, J., Wada, M., and Kuga, S. (2001). "Steric stabilization of a cellulose microcrystal suspension by poly(ethylene glycol) grafting," *Langmuir* 17(1), 21-27. https://doi.org/10.1021/la001070m

Badylak, S. F., and Gilbert, T. W. (2008). "Immune response to biologic scaffold materials," *Seminars in Immunology* 20(2), 109-116. https://doi.org/10.1016/j.smim.2007.11.003

Bock, N., Delbianco, M., Eder, M., Weinkamer, R., Amini, S., Bidan, C. M., Cipitria, A., Collin, S. P., Haupt, L. M., McGovern, J., Medeiros Savi, F., Toh, Y.-C., Hutmacher, D. W., and Fratzl, P. (2025). "A materials science approach to extracellular matrices," *Progress in Materials Science* 149, article 101391. https://doi.org/10.1016/j.pmatsci.2024.101391

Chau, M., De France, K. J., Kopera, B., Machado, V. R., Rosenfeldt, S., Reyes, L., Chan, K. J. W., Förster, S., Cranston, E. D., Hoare, T., and Kumacheva, E. (2016).

"Composite hydrogels with tunable anisotropic morphologies and mechanical properties," *Chemistry of Materials* 28(10), 3406-3415. https://doi.org/10.1021/acs.chemmater.6b00792

Chen, D., and van de Ven, T. G. M. (2016). "Flocculation kinetics of precipitated calcium carbonate (PCC) with sterically stabilized nanocrystalline cellulose (SNCC)," *Colloids and Surfaces A: Physicochemical and Engineering Aspects* 506, 789-793. https://doi.org/10.1016/j.colsurfa.2016.07.058

Chen, Y., Zhang, L., Yang, Y., Pang, B., Xu, W., Duan, G., Jiang, S., and Zhang, K. (2021). "Recent progress on nanocellulose aerogels: Preparation, modification, composite fabrication, applications," *Advanced Materials* 33(11), article 5569. https://doi.org/10.1002/adma.202005569

Chen, Z., Du, C., Liu, S., Liu, J., Yang, Y., Dong, L., Zhao, W., Huang, W., and Lei, Y. (2024). "Progress in biomaterials inspired by the extracellular matrix," *Giant* 19, article 100323. https://doi.org/10.1016/j.giant.2024.100323

Fang, Y., Han, E., Zhang, X.-X., Jiang, Y., Lin, Y., Shi, J., Wu, J., Meng, L., Gao, X., Griffin, P. J., Xiao, X., Tsai, H.-M., Zhou, H., Zuo, X., Zhang, Q., Chu, M., Zhang, Q., Gao, Y., Roth, L. K., Bleher, R., Ma, Z., Jiang, Z., Yue, J., Kao, C.-M., Chen, C.-T., Tokmakoff, A., Wang, J., Jaeger, H. M., and Tian, B. (2020). "Dynamic and programmable cellular-scale granules enable tissue-like materials," *Matter* 2(4), 948-964. https://doi.org/10.1016/j.matt.2020.01.008

De France, K. J., Hoare, T., and Cranston, E. D. (2017). "Review of hydrogels and aerogels containing nanocellulose," *Chemistry of Materials* 29(11), 4609-4631. https://doi.org/10.1021/acs.chemmater.7b00531

Habibi, Y., Lucia, L. A., and Rojas, O. J. (2010). "Cellulose nanocrystals: Chemistry, self-assembly, and applications," *Chemical Reviews* 110(6), 3479-3500. https://doi.org/10.1021/cr900339w

Hollister, S. J. (2005). "Porous scaffold design for tissue engineering," *Nature Materials* 4(7), 518-524. https://doi.org/10.1038/nmat1421

Jaberi, A., Xiang, Y., and Sheikhi, A. (2025). "Multiscale structure–property relationships in gelatin-based granular hydrogel scaffolds," *ACS Macro Letters* 14(10), 1569-1578. https://doi.org/10.1021/acsmacrolett.5c00441

Kim, U.-J., Kuga, S., Wada, M., Okano, T., and Kondo, T. (2000). "Periodate oxidation of crystalline cellulose," *Biomacromolecules* 1(3), 488-492. https://doi.org/10.1021/bm0000337

Koshani, R., Eiyegbenin, J. E., Wang, Y., and van de Ven, T. G. M. (2022). "Synthesis and characterization of hairy aminated nanocrystalline cellulose," *Journal of Colloid and Interface Science* 607, 134-144. https://doi.org/10.1016/j.jcis.2021.08.172

Koshani, R., Kheirabadi, S., and Sheikhi, A. (2025). "Nano-enabled dynamically responsive living acellular hydrogels," *Materials Horizons* 12(1), 103-118. https://doi.org/10.1039/D4MH00922C

Koshani, R., Yeh, S.-L., Pitcher, M. L., and Sheikhi, A. (2024). "Antiscaling Pickering emulsions enabled by amphiphilic hairy cellulose nanocrystals," *ACS Applied Materials & Interfaces* 16(32), 42802-42815. https://doi.org/10.1021/acsami.4c03451

Koshy, J. T., Sangeetha, D., V.P., A., Arthi, T. S., and Vijay, P. (2025). "Physically crosslinked freeze-thaw cryogels reinforced with functional nanocellulose derivatives (CM-CNFs) derived from biomass for wound dressing applications," *International Journal of Biological Macromolecules* 323, article 147185. https://doi.org/10.1016/j.ijbiomac.2025.147185

Modulevsky, D. J., Cuerrier, C. M., and Pelling, A. E. (2016). "Biocompatibility of subcutaneously implanted plant-derived cellulose biomaterials," *PLOS ONE*, (F. Zhao, ed.), 11(6), article e0157894. https://doi.org/10.1371/journal.pone.0157894

Ohshima, H. (1996). "Henry's function for electrophoresis of a cylindrical colloidal particle," *Journal of Colloid and Interface Science* 180(1), 299-301. https://doi.org/10.1006/jcis.1996.0305

OpenStax. (2016). "Infrared spectra of some common functional groups," in: *Organic Chemistry*, LibreTexts, <chem.libretexts.org/Bookshelves/Organic_Chemistry/Organic_Chemistry_(OpenStax)/12%3A_Structure_Determination__Mass_Spectrometry_and_Infrared_Spectroscopy/12.08%3A_Infrared_Spectra_of_Some_Common_Functional_Groups> (Jan. 30, 2026).

Pitcher, M. L., Koshani, R., and Sheikhi, A. (2024). "Chemical structure–property relationships in nanocelluloses," *Journal of Polymer Science* 62(1), 9-31. https://doi.org/10.1002/pol.20230558

Shakya, K. R., Nigam, K., Sharma, A., Jahan, K., Tyagi, A. K., and Verma, V. (2024). "Preparation and assessment of agar/TEMPO-oxidized bacterial cellulose cryogels for hemostatic applications," *Journal of Materials Chemistry B* 12(14), 3453-3468. https://doi.org/10.1039/D4TB00047A

Sheikhi, A., and van de Ven, T. G. M. (2017). "Colloidal aspects of Janus-like hairy cellulose nanocrystalloids," *Current Opinion in Colloid & Interface Science*, 29, 21-31. https://doi.org/10.1016/j.cocis.2017.02.001

Sun, B. (2021). "The mechanics of fibrillar collagen extracellular matrix," *Cell Reports Physical Science* 2(8), article 100515. https://doi.org/10.1016/j.xcrp.2021.100515

Tavakolian, M., Koshani, R., Tufenkji, N., and van de Ven, T. G. M. (2023). "Antibacterial Pickering emulsions stabilized by bifunctional hairy nanocellulose," *Journal of Colloid and Interface Science* 643, 328-339. https://doi.org/10.1016/j.jcis.2023.04.033

van de Ven, T. G. M., and Sheikhi, A. (2016). "Hairy cellulose nanocrystalloids: A novel class of nanocellulose," *Nanoscale* 8(33), 15101-15114. DOI: 10.1039/C6NR01570K

Wang, M., Jiang, G., Guo, X., Zeng, S., and Zhao, D. (2025). "Cellulose functional gels: Physical design and promising applications," *Advanced Physics Research* 4(6), article 20. https://doi.org/10.1002/apxr.202500020

Yamada, K. M., Doyle, A. D., and Lu, J. (2022). "Cell-3D matrix interactions: Recent advances and opportunities," *Trends in Cell Biology* 32(10), 883-895. https://doi.org/10.1016/j.tcb.2022.03.002

Yang, H., Chen, D., and van de Ven, T. G. M. (2015). "Preparation and characterization of sterically stabilized nanocrystalline cellulose obtained by periodate oxidation of cellulose fibers," *Cellulose* 22(3), 1743-1752. https://doi.org/10.1007/s10570-015-0584-4

Yang, H., Sheikhi, A., and van de Ven, T. G. M. (2016). "Reusable green aerogels from cross-linked hairy nanocrystalline cellulose and modified chitosan for dye removal," *Langmuir* 32(45), 11771-11779. https://doi.org/10.1021/acs.langmuir.6b03084

Yang, X., and Cranston, E. D. (2014). "Chemically cross-linked cellulose nanocrystal aerogels with shape recovery and superabsorbent properties," *Chemistry of Materials* 26(20), 6016-6025. https://doi.org/10.1021/cm502873c

Zhao, T., Huang, Y., Zhu, J., Qin, Y., Wu, H., Yu, J., Zhai, Q., Li, S., Qin, X., Wang, D., Li, T., and Liu, Y. (2025). "Extracellular matrix signaling cues: Biological functions, diseases, and therapeutic targets," *MedComm* 6(8), article e70281. https://doi.org/10.1002/mco2.70281

Article submitted: February 7, 2026; Peer review completed: March 7, 2026; Revised version received and accepted: May 6, 2026; Published: May 27, 2026.
DOI: 10.15376/biores.21.3.6416-6435

APPENDIX

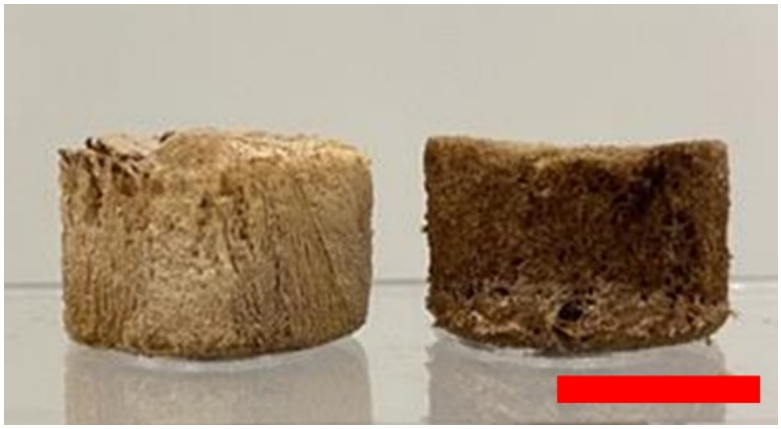


Fig. A1. Images of BHCNC/DAmC cryogels at a ~ 1:1 (left) or ~ 1:3 (right) –CHO:–NH_2 molar ratio. Scale bar is 1 cm.

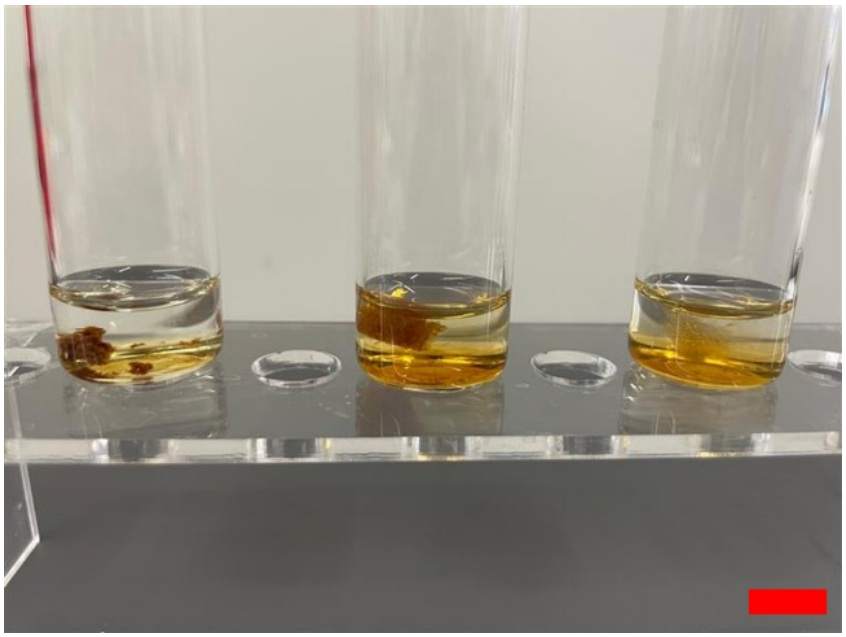


Fig. A2. Photographs of BHCNC/DAmC cryogels at varying functional group molar ratios (left, ~ 3:1, middle, ~ 1:1, and right, ~ 1:3) after incubation in ultrapure water for 3 months, demonstrating the long-term stability of cryogels. Scale bar is 1 cm.

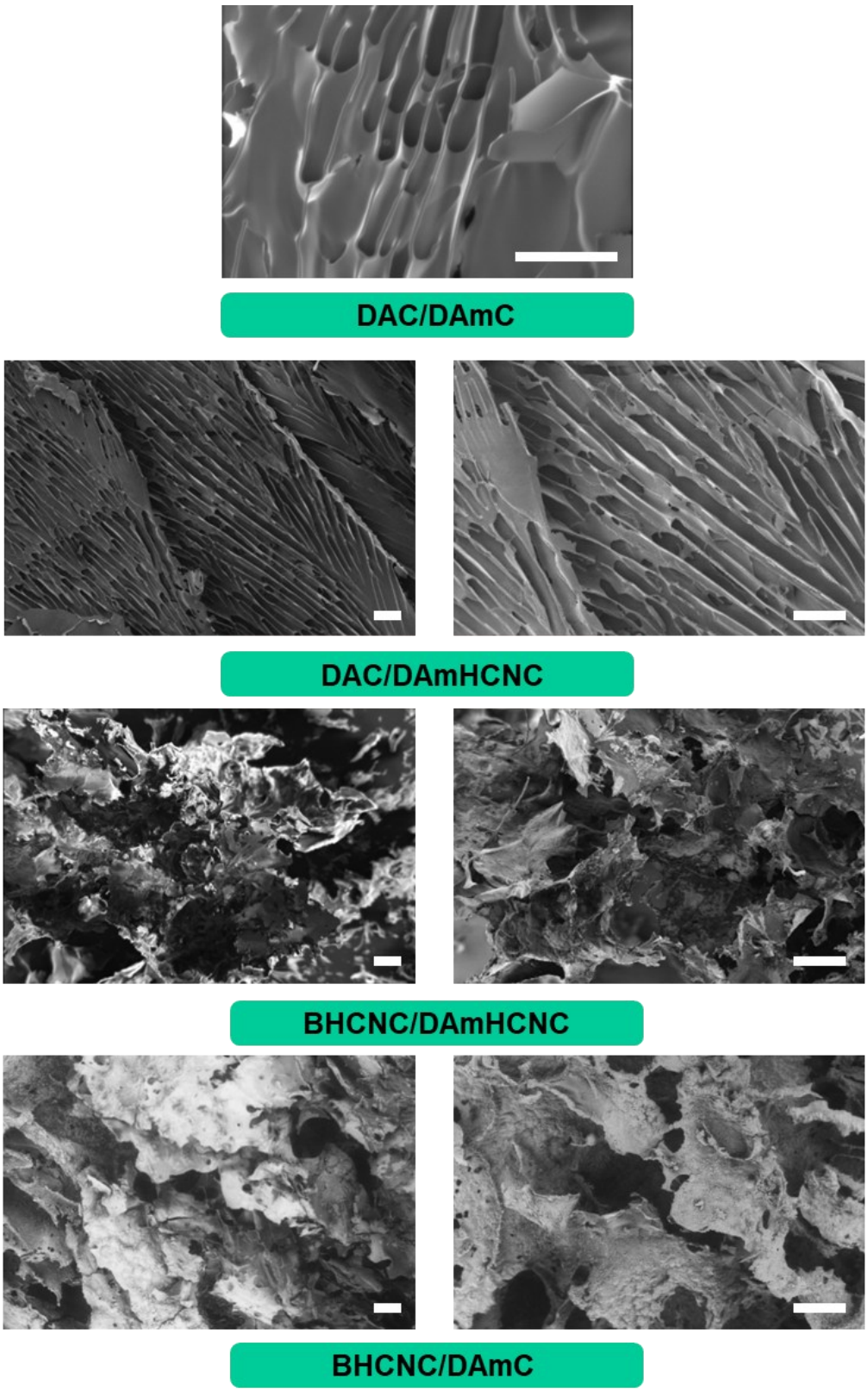


Fig. A3. SEM images of cryogels at a constant ~ 3:1 –CHO:–NH_2 molar ratio, demonstrating varying microstructures. Scale bars are 100 µm.